DOI: 10.1002/ejic.200501155

Hydrothermal Syntheses, Architectures and Magnetic Properties of Six Novel Mn^{II} Coordination Polymers with Mixed Ligands

Chang-Yan Sun,[a] Song Gao,*[b] and Lin-Pei Jin*[a]

Keywords: Coordination polymers / Magnetic properties / Manganese / Microporous materials / Organic–inorganic hybrid composites

Six novel manganese(II) coordination polymers, namely $[Mn(oba)(4,4'\text{-bpy})]_n \cdot n(4,4'\text{-bpy})$ (**1**), $[Mn(oba)(phen)(H_2O)]_n$ (**2**), $[Mn_2(oba)_2(2,2'\text{-bpy})_2(H_2O)_2]_n \cdot nH_2oba$ (**3**), $[Mn_2(cca)_2(4,4'\text{-bpy})_2]_n \cdot 2n(4,4'\text{-bpy})$ (**4**), $[Mn(cca)(phen)]_n$ (**5**) and $[Mn(cca)(2,2'\text{-bpy})]_n \cdot 0.25nH_2O$ (**6**) [H_2oba = 4,4′-oxybis(benzoic acid); 4,4′-bpy = 4,4′-bipyridine; phen = 1,10-phenanthroline; 2,2′-bpy = 2,2′-bipyridine; H_2cca = *p*-carboxycinnamic acid] have been synthesised under hydrothermal conditions. Complexes **1** and **4** possess 3D microporous metal-organic frameworks with free 4,4′-bpy ligands in the channels. The Mn^{II} ions in complex **2** are bridged into 1D infinite double-chain structures, and those in complex **3** are bridged into 1D zigzag chains. Hydrogen bonds cause the formation of 3D supramolecular networks for complexes **2** and **3**. Complex **5** is a complicated 3D metal-organic framework, and the Mn^{II} ions in complex **6** are linked into 2D layers with cavities; interpenetration of these 2D layers results in the formation of a 3D supramolecular network. Magnetic susceptibility measurements indicate that complex **2** displays a weak ferromagnetic interaction between the Mn^{II} ions with the following parameters: J = 0.462(3) cm^{-1}, g = 2.0387(6), zJ' = –0.0062(3) cm^{-1} and $R = 8.0 \times 10^{-6}$. Complex **4** shows antiferromagnetic coupling between the Mn^{II} ions with J = –0.718(4) cm^{-1}, g = 1.986(4) and $R = 2.3 \times 10^{-4}$.

Introduction

Manganese-based coordination compounds have received considerable interest in the fields of supramolecular chemistry, crystal engineering and materials chemistry. This interest arises not only from their remarkable magnetochemical properties,[1] but also from their rich biochemistry.[2] Furthermore, due to their low cost and toxicity, manganese coordination compounds are growing in importance as homogeneous catalysts.[3] As far as we know, the current focus is on the construction of molecule-based magnetic materials. The main approach is to employ short bridging ligands to connect manganese ions. These short ligands, such as azide,[4] cyanide[5] and oxalate,[6] efficiently mediate the magnetic coupling. Long bridging ligands, because of their large separation and thus their inefficiency in transmitting magnetic interactions, have seldom been used to construct manganese coordination compounds.

It is well-known that the topology of coordination compounds depends both on the coordination geometry of the metal centres and on the coordination behaviour of the organic ligands. When long bridging ligands are used to connect metal ions, their versatile coordination modes may lead to new architectures with novel topologies and interesting properties.

4,4′-Oxybis(benzoic acid) (H_2oba) is a typical example of long V-shaped ligands. Its coordination chemistry has been studied and some coordination polymers have been obtained.[7] Because of its two oxo carboxylate groups, H_2oba can coordinate to metal ions in didentate, tridentate, tetradentate, pentadentate and hexadentate modes. *p*-Carboxycinnamic acid (H_2cca) also has two oxo carboxylate groups. There is only one cobalt(II) complex known with H_2cca,[8] and we are interested in the architecture of metal complexes with this asymmetrical functional carboxylate ligand.

The choice of a suitable co-ligand often has a significant effect on the formation and structure of metal complexes. 4,4′-Bipyridine (4,4′-bpy) has been demonstrated to be one of the most important rigid linear co-ligands and has been extensively used to connect metal ions.[9] Chelating N-containing aromatic ligands, such as 2,2′-bipyridine (2,2′-bpy) and 1,10-phenanthroline (phen), can not only affect the coordination geometry of metal ions but also bring about π-π stacking interactions, which are important for the construction of supramolecular networks.[10]

Taking into account the above-mentioned aspects, we report here the syntheses, structures and magnetic properties

[a] School of Chemistry, Beijing Normal University, Beijing 100875, P. R. China
Fax: +86-105-880-2075
E-mail: lpjin@bnu.edu.cn
[b] State Key Laboratory of Rare Earth Materials Chemistry and Applications, College of Chemistry and molecular Engineering, Peking University, Beijing 100871, P. R. China
Supporting information for this article is available on the WWW under http://www.eurjic.org or from the author.

of six novel Mn^{II} coordination compounds, namely $[Mn(oba)(4,4'\text{-bpy})]_n \cdot n(4,4'\text{-bpy})$ (**1**), $[Mn(oba)(phen)(H_2O)]_n$ (**2**), $[Mn_2(oba)_2(2,2'\text{-bpy})_2(H_2O)_2]_n \cdot nH_2oba$ (**3**), $[Mn_2(cca)_2\ (4,4'\text{-bpy})_2]_n \cdot 2n(4,4'\text{-bpy})$ (**4**), $[Mn(cca)(phen)]_n$ (**5**) and $[Mn(cca)(2,2'\text{-bpy})]_n \cdot 0.25nH_2O$ (**6**). All six coordination polymers contain long spacers (oba/cca) and co-ligands (4,4′-bpy/phen/2,2′-bpy), and possess very different structures, ranging from 1D chains to 2D layers and 3D metal-organic frameworks.

Results and Discussion

Description of the Structures

[Mn(oba)(4,4′-bpy)]$_n$·n(4,4′-bpy) (1)

Complex **1** is a 3D porous coordination polymer containing channels with guest 4,4′-bpy molecules. There is only one metal environment in complex **1**, as shown in Figure 1. Each Mn^{II} ion is coordinated to four oxygen atoms of four oba ligands and two nitrogen atoms of two 4,4′-bpy ligands, and is located in a slightly distorted octahedral geometry. The average Mn–N bond length is 2.322 Å and the Mn–O bond lengths are in the range 2.147–2.162 Å. Each oba ligand in complex **1** is severely bent at the ether-oxygen site (C–O–C = 118.6°) and adopts a bis(bridging didentate) mode, linking four Mn^{II} ions (see Scheme 1a). All Mn^{II} ions are connected by oba ligands into 2D pillar-like layers. The nearest Mn···Mn distance in these layers is 4.835 Å. The 4,4′-bpy ligands bridge these layers into a 3D porous framework with channels of about 11 × 14 Å (based on the distance between metal ions), as shown in Figure 2. The channels are big enough to accommodate free 4,4′-bpy molecules.

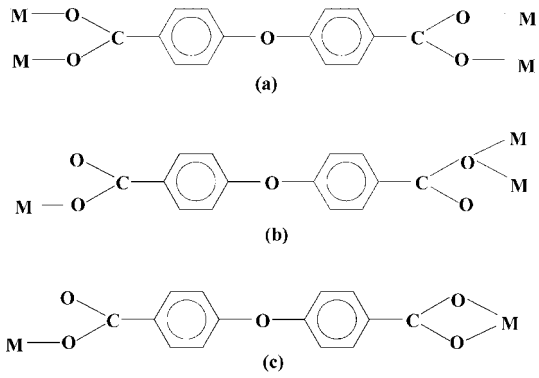

Scheme 1. The coordination modes of the oba ligands in complexes **1**–**3**.

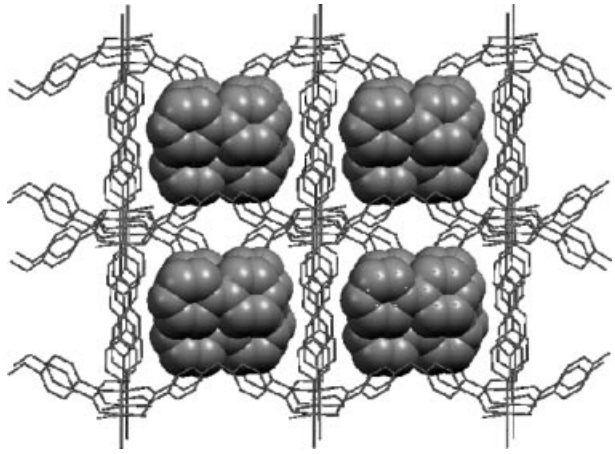

Figure 2. The 3D porous framework of complex **1** viewed along the *c* axis, with space-filling models representing the free 4,4′-bpy molecules.

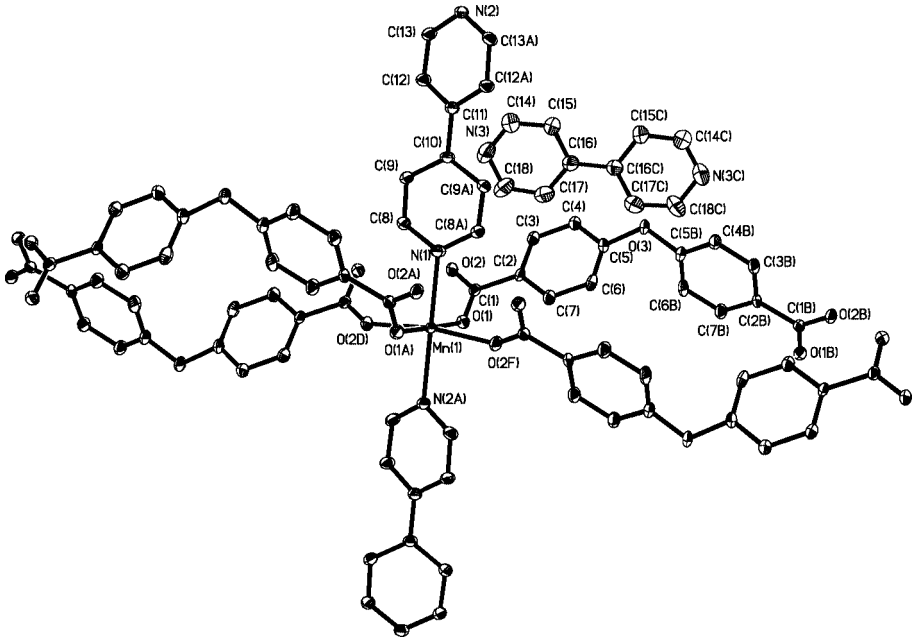

Figure 1. The coordination environment of the Mn^{II} ion in complex **1** with 30% thermal ellipsoids. All hydrogen atoms have been omitted for clarity.

[Mn(oba)(phen)(H_2O)]$_n$ (2)

Figure 3 shows the coordination environment of the Mn^{II} ions in complex **2**. The coordination geometry around each Mn^{II} ion is N_2O_4, with three oxygens from three oba ligands, one oxygen from a coordinated water molecule and two nitrogens from one phen ligand, and can be described as a distorted octahedron. The average Mn–N bond length is 2.271 Å and the Mn–O bond lengths are in the range 2.107–2.158 Å. The oba ligands are also bent (C–O–C: 118.6°), as in complex **1**. The coordination modes in complexes **1** and **2**, however, are different as each oba ligand in complex **2** adopts a tridentate mode, linking three Mn^{II} ions, as shown in Scheme 1b. This coordination mode has not been reported before. The bridging carboxylate oxygen atoms cause the formation of the building blocks of Mn_2O_2 cores, in which the Mn···Mn distance is 3.387 Å (Mn–O–Mn angle: 101.81°). These cores are interconnected by oba ligands into 1D double-chain structures. A similar structure has been reported for [Zn(bpndc)(phen)(H_2O)]$_n$.[11] There are hydrogen bonds between the coordinated water molecules and the uncoordinated carboxylate oxygen atoms (O···O distances of 2.697 and 2.740 Å). In addition, weak π-π stacking interactions exist between phen molecules of neighbouring chains, with an average distance of 3.53 Å. Both the hydrogen bonds and π-π stacking interactions result in the formation of a 3D supramolecular network with channels of about 3 × 13 Å. This is small and means that it is unable to incorporate any guest molecules.

[Mn_2(oba)$_2$(2,2′-bpy)$_2$(H_2O)$_2$]$_n$·nH_2oba (3)

There are two kinds of crystallographically different Mn^{II} ions in complex **3**, as shown in Figure 4. Both Mn(1) and Mn(2) are coordinated to three oxygen atoms of two oba ligands, one from a coordinated water molecule and two nitrogen atoms of a 2,2′-bpy ligand, but their bond lengths and bond angles are different. The average Mn(1)–N bond length is 2.261 Å and the Mn(1)–O bond lengths are in the range 2.085–2.408 Å, while the average Mn(2)–N bond length is 2.242 Å and the Mn(2)–O bond lengths are in the range 2.095–2.363 Å. Mn(1) and Mn(2) are bridged by an oba ligand with a distance of 14.365 Å. There are three kinds of oba ligands in complex **3**, two of which coordinate in a tridentate mode linking two Mn^{II} ions (see Scheme 1c). They are bent at the ether-oxygen sites (C–O–C = 118.4° and 119.9°), and connect the Mn^{II} ions into 1D infinite zigzag chains (the Mn···Mn distance within a chain is 14.365 Å). The third kind of oba ligand is protonated and does not coordinate to Mn^{II}. It is also bent at the ether-oxygen sites, with a C–O–C angle of 120.2°. There are hydrogen bonds between the coordinated water molecules and the coordinated oba/free H_2oba ligands (O···O distances of

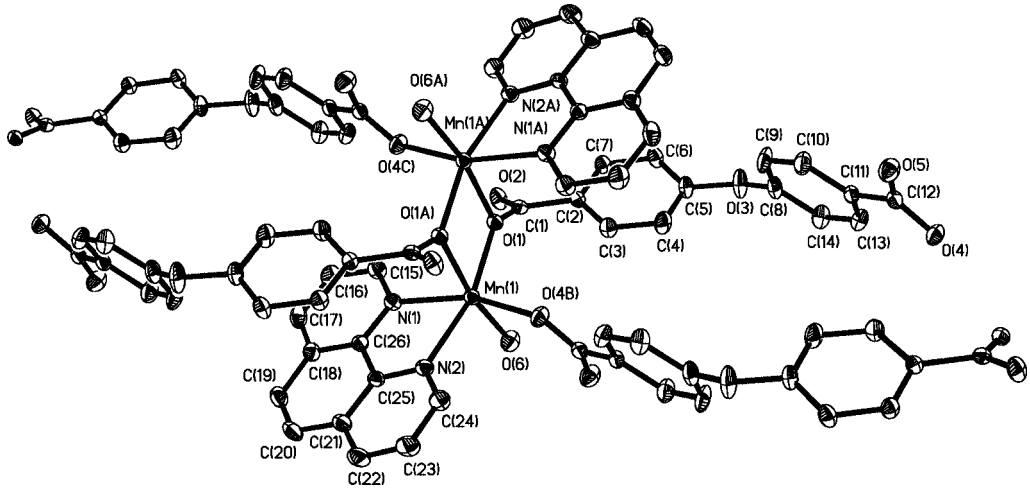

Figure 3. The coordination environment of the Mn^{II} ion in complex **2** with 30% thermal ellipsoids. All hydrogen atoms have been omitted for clarity.

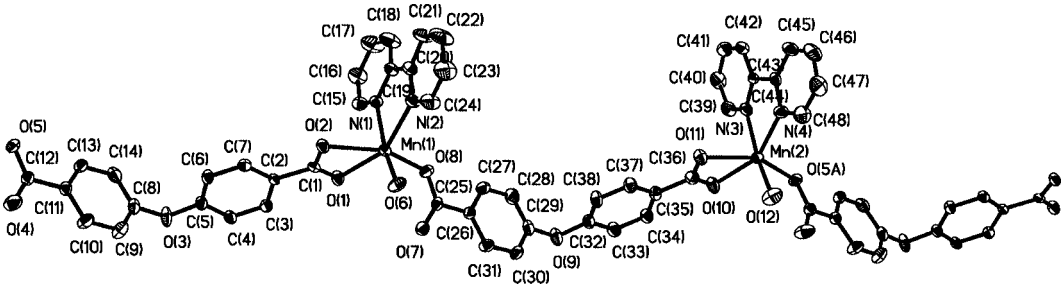

Figure 4. The coordination environments of the Mn^{II} ions in complex **3** with 30% thermal ellipsoids. Free H_2oba ligands and all hydrogen atoms have been omitted for clarity.

2.896, 2.753 and 2.855 Å), forming a 3D supramolecular network, as shown in Figure 5.

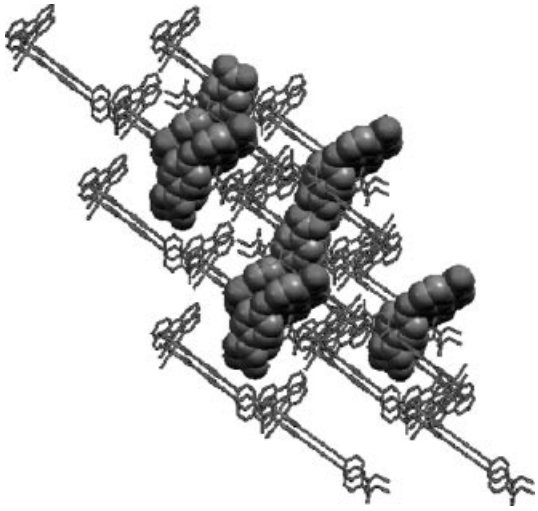

Figure 5. The 3D supramolecular network of complex **3** viewed along the *a* axis, with space-filling models representing the free H_2oba ligands.

[Mn$_2$(cca)$_2$(4,4′-bpy)$_2$]$_n$·2n(4,4′-bpy) (4)

Complex **4** possesses a 3D porous metal-organic framework whose channels contain free 4,4′-bpy molecules. Similar to complex **3**, there are two types of Mn^{II} environments (see Figure 6). Both Mn(1) and Mn(2) are coordinated to four oxygen atoms of four cca ligands and two nitrogen atoms of two 4,4′-bpy molecules, and are located in slightly distorted octahedra. However, their bond lengths and angles are different. The Mn(1)–N bond length is 2.275 Å and the Mn(1)–O bond lengths are in the range 2.152–2.173 Å, while the Mn(2)–N bond length is 2.299 Å and the Mn(2)–O bond lengths are in the range 2.166–2.197 Å. Mn(1) and Mn(2) are bridged by two carboxylate groups of two cca ligands with a distance of 5.112 Å. Each cca ligand in complex **4** adopts a tetradentate mode, linking four Mn^{II} ions (see Scheme 2a). All Mn^{II} ions are connected by cca ligands into 2D pillar-like layers. These layers are interconnected by 4,4′-bpy ligands, resulting in the formation of a 3D porous framework with channels of about 11 × 11 Å, similar to those in complex **1**. These channels contain free 4,4′-bpy molecules.

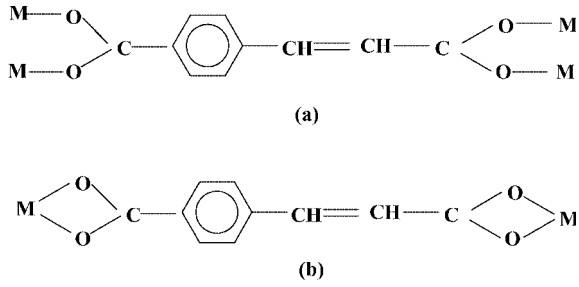

Scheme 2. The coordination modes of the cca ligands in complexes **4**–**6**.

[Mn(cca)(phen)]$_n$ (5)

There is only one metal environment in complex **5**, as shown in Figure 7. Each Mn^{II} ion is placed in a distorted octahedron, which is completed by four oxygen atoms of four cca ligands and two nitrogen atoms of one phen molecule with the same Mn–N distance. The Mn–N bond length is 2.317 Å and the Mn–O bond lengths are in the range 2.094–2.203 Å. Each cca ligand adopts a tetradentate mode, linking four Mn^{II} ions (see Scheme 2a). The nearest Mn···Mn distance is 4.587 Å. All Mn^{II} ions are linked by cca ligands into a 3D metal-organic framework with 1D channels. However, chelating phen ligands occupy the diagonal position, which greatly decreases the dimension of the

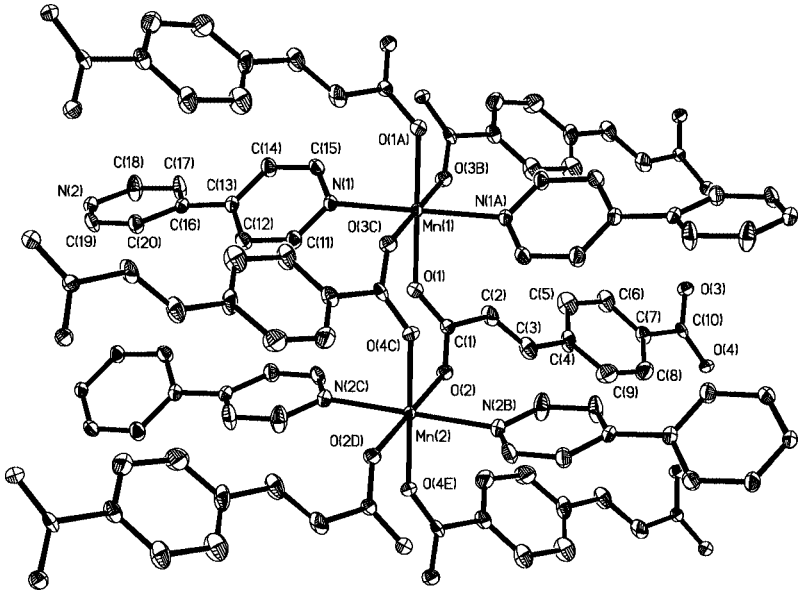

Figure 6. The coordination environments of the Mn^{II} ions in complex **4** with 30% thermal ellipsoids. All hydrogen atoms have been omitted for clarity.

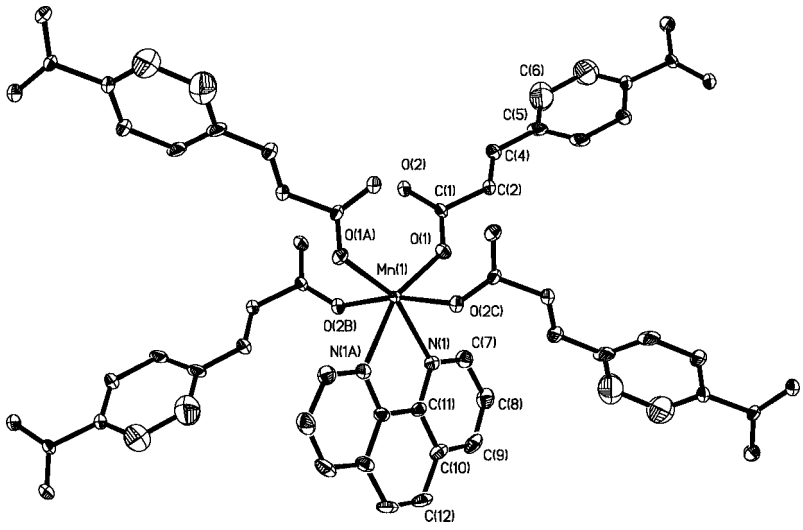

Figure 7. The coordination environment of the Mn^{II} ion in complex **5** with 30% thermal ellipsoids. All hydrogen atoms have been omitted for clarity.

channels. All phen rings are parallel to each other, and the nearest face-to-face distance is 3.29 Å, indicating the presence of π-π stacking interactions.

[Mn(cca)(2,2′-bpy)]$_n$·0.25nH_2O (6)

Because of the disorder of the cca ligands, there are four types of Mn^{II} environment. Figure 8 shows one of them, and the others can be found in the Supporting Information (Figures S1–S3). Each Mn^{II} ion is coordinated to four oxygen atoms of three cca ligands and two nitrogen atoms of one 2,2′-bpy molecule. The cca ligands in complex **6** adopt two kinds of coordination modes, namely bis(bridging didentate) and bis(chelating didentate) (see Scheme 2). The dinuclear species $[Mn_2(cca)_2(2,2'\text{-bpy})_2]$, which has a metal–metal distance of 4.462 Å, can be regarded as a secondary building block. These moieties are linked by cca ligands into 2D grid-like layers with cavities of about 12 × 13 Å, and the 2D layers are interpenetrated, resulting in the formation of a 3D supramolecular network in which weak π-π stacking interactions between 2,2′-bpy molecules (the nearest distance is 3.29 Å) further stabilize the supramolecular structure.

It is obvious from the above descriptions that the carboxylate ligands and the co-ligands have significant effects on the formation and architecture of the resulting complexes. The structures of these six complexes can be simplified as shown in Scheme 3. Although complexes **1**, **2** and **3** contain the same carboxylate ligand oba, they possess different structures. In complex **1**, both V-shaped oba and linear 4,4′-bpy ligands work as bridging ligands, resulting in the formation of a 3D porous structure. The free 4,4′-bpy ligands may be one of the important factors for the construction of the porous structure as they might function as templates and occupy the pores, thus preventing further interpenetration. Complexes **2** and **3** possess infinite 1D chains, which may be attributed to the existence of the terminal ligands phen/2,2′-bpy/H_2O. These terminal ligands occupy the coordination sites of the metal ions and prevent the

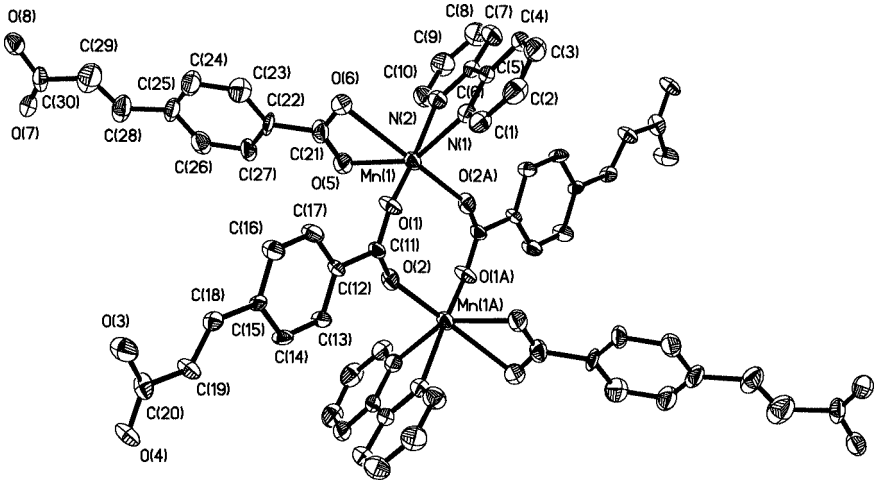

Figure 8. The coordination environment of the Mn^{II} ion in complex **6** with 30% thermal ellipsoids. All hydrogen atoms have been omitted for clarity.

structures from extending into higher dimensions. Complex **2** has a double-chain structure while complex **3** has a single-chain structure because the oba ligands adopt different coordination modes in the two complexes (see Scheme 1 i and b). When the oba ligand is replaced by cca, we obtain the box-like structure of complex **4**. Both cca and 4,4′-bpy are bridging ligands that link metal ions into a 3D porous structure. The presence of free 4,4′-bpy works as template, promoting the formation of the 3D porous structure. However, with the terminal ligand phen, complex **5** possesses a 3D metal-organic framework due to the tetradentate bridging ligand cca, and in complex **6** the introduction of 2,2′-bpy as a ligand leads to 2D grid-like layers, where hydrogen bond and π-π stacking interactions result in a 3D supramolecular network.

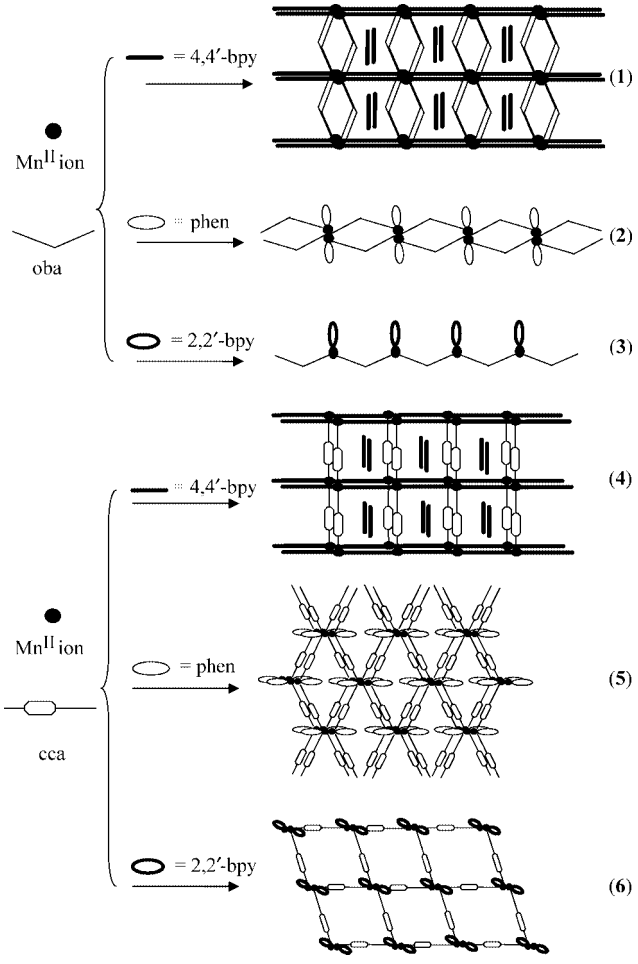

Scheme 3. A simplified representation of the structures of complexes **1**–**6**.

Both oba and cca have two *exo* carboxylate groups, but there are some differences in their complexes. Comparing complexes **1** and **4**, although they are both 3D porous structures they are quite different: complex **1** possesses dumbbell-like channels while complex **4** possesses regular rhombus channels. This is because oba is V-shaped whereas cca is nearly linear. The introduction of phen and 2,2′-bpy as ligands in the Mn^{II}/oba and Mn^{II}/cca systems results in different structures. Complexes **2** and **3** are infinite 1D chains, while complex **5** possesses a complicated 3D structure and complex **6** is made up of 2D grid-like layers when only coordination bonds are considered. The existence of coordinated water molecules in complexes **2** and **3** is one important factor for the formation of the chain structures. The V-shaped oxo carboxylate ligand oba is also fundamental for the construction of chains in the presence of terminal ligands such as phen and 2,2′-bpy,[7a,7b,7e] while the linear ligand cca contributes to higher dimensionalities in complexes **5** and **6**, thus showing that the shape of the ligands plays an important role in the architecture of coordination polymers.

Magnetic Properties

Magnetic Properties of Complex 2

The χ_m^{-1} and $\chi_m T$ vs. T plots (2–300 K) of complex **2** are shown in Figure 9. The magnetic susceptibility data (10 to 300 K) of complex **2** obey the Curie–Weiss law very well, with a Weiss constant, θ, of +3.2 K and a Curie constant, C, of 4.554(1) $cm^3 K mol^{-1}$. The value of C is consistent with one spin-only Mn^{II} ion with $S = 5/2$ and $g = 2.040$. The positive Weiss constant and the increase of $\chi_m T$ upon cooling are typical of a ferromagnetic coupling between the Mn^{II} ions. Based on the structural data, the magnetic susceptibility data of complex **2** can be analysed by using a Mn_2 dimer model with an intradimer interaction J and including the contribution of the intermolecular interaction zJ'. Assuming an isotropic exchange, the exchange Hamiltonian $H = -2JS_1S_2$, with $S_1 = S_2 = 5/2$, and the expression for magnetic susceptibility may be used to fit the data.[12] The least-squares fit of the experimental data in the whole temperature range gives the following parameters: J = 0.462(3) cm^{-1}, g = 2.0387(6), zJ' = –0.0062(3) cm^{-1}, and $R = 8.0 \times 10^{-6}$.

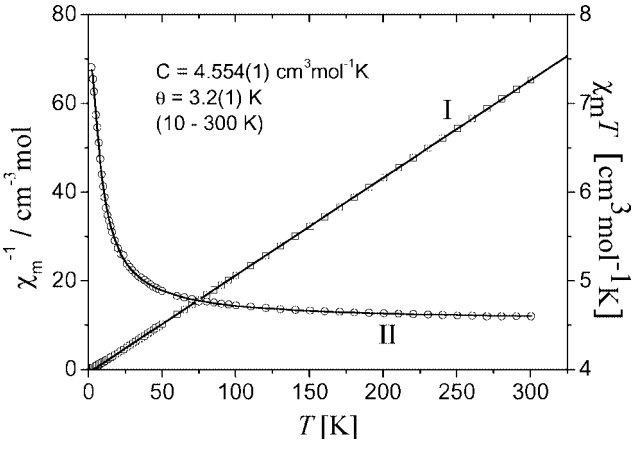

Figure 9. Temperature dependence of χ_m^{-1} and $\chi_m T$ for complex **2**. Line I is the fit of the Curie–Weiss law and line II is the fit using a dimer model (see text).

Clearly, a weak ferromagnetic interaction is observed in the doubly (μ-O)-carboxylate bridged Mn^{II} dimer, while some structurally similar Mn^{II} dimers show weak antiferromagnetic coupling between the Mn^{II} ions (Table 1).[13] The ferromagnetic coupling in complex **2** may be mainly due to the smaller Mn–O–Mn angle, which facilitates ferromagnetic coupling as in some azido- or chloro-bridged Mn^{II} dimers.[14]

Table 1. Comparison of the magnetic coupling constant J and structural parameters for $Mn^{II}_2(\mu\text{-}O)_2$ complexes.

Compd.	J [cm^{-1}]	Mn···Mn [Å]	Mn–O–Mn [°]	Ref.
A	–0.631	3.712(2)	109.1(3), 109.8(3)	[13a]
B	–0.655	3.726(4)	108.9(3)	[13a]
C	–0.785	3.460(1)	105.04(7), 102.77(7)	[13b]
D	+0.462	3.387(12)	101.81(7)	this work

Magnetic Properties of Complex 3

The χ_m^{-1} and $\chi_m T$ vs. T plots (2–300 K) of complex **3** are shown in Figure 10. The magnetic susceptibility data (2 to 300 K) of complex **3** obey the Curie–Weiss law very well with a very small Weiss constant of 0.09 K and a Curie constant of 9.004(1) $cm^3\,K\,mol^{-1}$. The value of C is consistent with two non-interacting spin-only Mn^{II} ions with S = 5/2 and g = 2.029. The very small Weiss constant suggests essentially no magnetic coupling between the Mn^{II} ions, which is consistent with the long separation between the Mn^{II} ions in this complex. The peak around 50 K might arise from the effect of oxygen.[15]

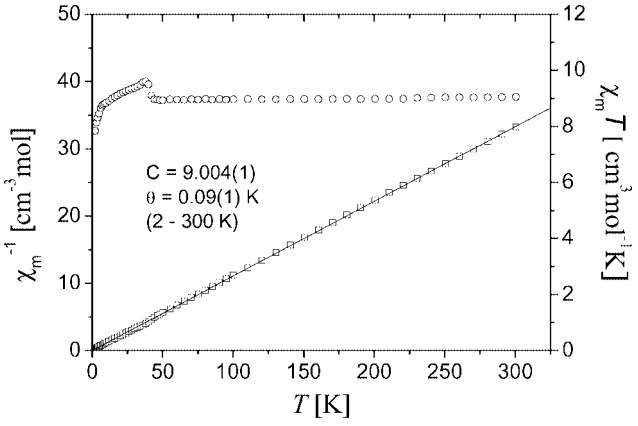

Figure 10. Temperature dependence of χ_m^{-1} and $\chi_m T$ for complex **3**. The line is the fit of the Curie–Weiss law.

Magnetic Properties of Complex 4

The χ_m^{-1} and χ_m vs. T plots (2–300 K) of complex **4** are shown in Figure 11. The magnetic susceptibility data (20 to 300 K) of complex **4** obey the Curie–Weiss law very well with a Weiss constant of –15.8 K and a Curie constant of 8.8355(7) $cm^3\,K\,mol^{-1}$. The value of C is consistent with two non-interacting spin-only Mn^{II} ions with S = 5/2 and g = 2.0098. The negative Weiss constant and the peak in the χ_m curve for the complex are typical of antiferromagnetic coupling between the Mn^{II} ions. Based on the structural data, complex **4** can be viewed as a 1D uniform chain along the a axis. Consequently, the magnetic susceptibility data of complex **4** can be analysed by using a 1D Fisher model with an intradimer interaction J. Assuming isotropic exchange, the exchange Hamiltonian is $H = -2JS_iS_j$ with $S_i = S_j$ = 5/2 and the expression of magnetic susceptibility may be used to fit the data.[16] The least-squares fit of the experimental data in the whole temperature range gives the following parameters: J = –0.718(4) cm^{-1}, g = 1.986(4), and $R = 2.3 \times 10^{-4}$. The J value falls in the range for other carboxylato-bridged Mn^{II} compounds.[17]

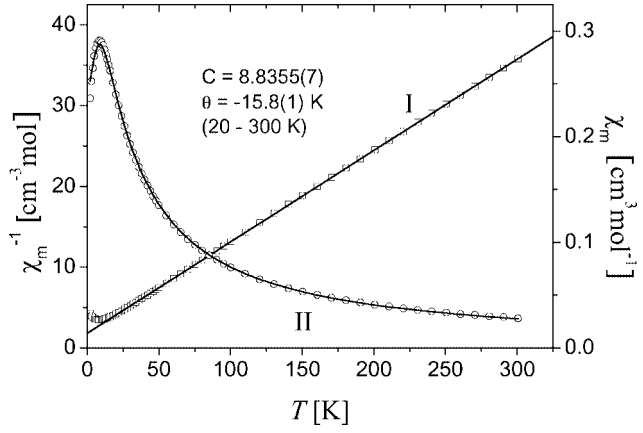

Figure 11. Temperature dependence of χ_m^{-1} and χ_m for complex **4**. Line I is the fit of the Curie–Weiss law and line II is the fit using a 1D Fisher model.

Conclusions

In summary, microporous Mn^{II} coordination polymers (complexes **1** and **4**) are formed by using the V-shaped ligand oba or the linear ligand cca with the rigid ligand 4,4′-bpy. The free 4,4′-bpy ligand acts as a template and also occupies the pore, thus preventing interpenetration. The introduction of terminal ligands such as 2,2′-bpy and phen leads to the formation of 1D chains for complexes **2** and **3**; hydrogen bonds mould these chains into 3D supramolecular networks. In complex **6**, the Mn^{II} ions are coordinated by cca and 2,2′-bpy into 2D layers that interpenetrate to form a 3D supramolecular network. A weak ferromagnetic interaction is observed in the doubly (μ-O)-carboxylate-bridged Mn^{II} dimer in complex **2**, which may be mainly due to the smaller Mn–O–Mn angle.

Experimental Section

General Remarks: All reagents were used as received without further purification. The C, H, N microanalyses were carried out with a Vario EL elemental analyzer. The IR spectra were recorded with a Nicolet Avatar 360 FT-IR spectrometer using the KBr pellet technique. The magnetic susceptibilities were obtained for crystalline

Table 2. Crystal data and structure refinement parameters for complexes **1**–**6**.

	1	**2**	**3**	**4**	**5**	**6**
Chemical formula	$C_{34}H_{24}MnN_4O_5$	$C_{26}H_{18}MnN_2O_6$	$C_{62}H_{46}Mn_2N_4O_{17}$	$C_{60}H_{44}Mn_2N_8O_8$	$C_{24}H_{14}N_2O_4Mn$	$C_{20}H_{14.50}MnN_2O_{4.25}$
Crystal system	monoclinic	triclinic	triclinic	triclinic	monoclinic	monoclinic
Space group	*P*2/*c*	$P\bar{1}$	$P\bar{1}$	$P\bar{1}$	*C*2/*c*	*C*2/*c*
Formula weight	623.51	509.36	1228.91	1114.91	449.31	405.78
a [Å]	13.251(4)	7.699(2)	11.317(4)	10.224(2)	21.897(7)	15.009(2)
b [Å]	11.742(4)	11.671(4)	16.036(5)	11.723(2)	11.677(4)	19.383(2)
c [Å]	9.317(3)	13.477(4)	17.986(6)	12.227(2)	7.396(2)	13.926(2)
α [°]	90	82.295(5)	64.910(6)	65.980(3)	90	90
β [°]	90.195(7)	83.799(5)	87.609(6)	71.305(3)	100.311(6)	114.709(2)
γ [°]	90	73.086(5)	76.789(6)	84.622(4)	90	90
V [Å^3]	1449.6(8)	1145.1(6)	2872.3(16)	1266.7(4)	1860.6(10)	3680.8(8)
Z	2	2	2	1	4	8
F(000)	642	522	1264	574	916	1660
D_c [g cm^{-3}]	1.428	1.477	1.421	1.462	1.604	1.464
T [K]	293(2)	293(2)	293(2)	293(2)	293(2)	293(2)
θ range [°]	1.73–26.39	2.26–26.43	1.25–25.01	1.90–25.01	1.89–26.49	1.83–26.35
μ [mm^{-1}]	0.506	0.623	0.516	0.566	0.747	0.747
GOF	1.025	1.042	1.003	1.013	1.127	1.046
Final *R* indices	R_1 = 0.0544	R_1 = 0.0408	R_1 = 0.0593	R_1 = 0.0509	R_1 = 0.0573	R_1 = 0.0360
[$I > 2\sigma(I)$]	wR_2 = 0.1118	wR_2 = 0.0934	wR_2 = 0.1392	wR_2 = 0.1140	wR_2 = 0.1600	wR_2 = 0.0838

Table 3. Selected bond lengths [Å] and angles [°] for complexes **1**–**3**.

1[a]			
Mn(1)–O(1)	2.162(2)	Mn(1)–N(1)	2.333(4)
Mn(1)–O(2)#1	2.147(2)	Mn(1)–N(2)#4	2.311(4)
O(1)–Mn(1)–N(1)	89.08(6)	O(2)#2–Mn(1)–O(1)	86.48(9)
O(1)–Mn(1)–N(2)#4	90.92(6)	O(2)#1–Mn(1)–N(1)	94.41(6)
O(1)#3–Mn(1)–O(1)	178.16(13)	O(2)#1–Mn(1)–N(2)#4	85.59(6)
O(2)#1–Mn(1)–O(1)	93.66(9)	N(2)#4–Mn(1)–N(1)	180.0
O(2)#1–Mn(1)–O(2)#2	171.18(12)		
2[b]			
Mn(1)–O(1)	2.156(2)	Mn(1)–O(6)	2.159(2)
Mn(1)–O(1)#2	2.208(2)	Mn(1)–N(1)	2.251(2)
Mn(1)–O(4)#1	2.107(2)	Mn(1)–N(2)	2.290(2)
O(1)–Mn(1)–O(1)#2	78.19(7)	O(4)#1–Mn(1)–O(6)	87.36(7)
O(1)–Mn(1)–O(6)	91.32(7)	O(4)#1–Mn(1)–N(2)	88.55(7)
O(1)–Mn(1)–N(1)	95.32(7)	O(4)#1–Mn(1)–N(1)	161.31(7)
O(1)–Mn(1)–N(2)	164.77(7)	O(6)–Mn(1)–O(1)#2	169.16(7)
O(1)#2–Mn(1)–N(1)	91.55(7)	O(6)–Mn(1)–N(1)	92.13(7)
O(1)#2–Mn(1)–N(2)	92.05(7)	O(6)–Mn(1)–N(2)	98.78(7)
O(4)#1–Mn(1)–O(1)	103.36(7)	N(1)–Mn(1)–N(2)	73.06(7)
O(4)#1–Mn(1)–O(1)#2	92.39(7)		
3[c]			
Mn(1)–O(1)	2.157(3)	Mn(2)–O(5)#1	2.095(4)
Mn(1)–O(2)	2.407(3)	Mn(2)–O(10)	2.179(4)
Mn(1)–O(6)	2.176(4)	Mn(2)–O(11)	2.363(4)
Mn(1)–O(8)	2.085(4)	Mn(2)–O(12)	2.176(4)
Mn(1)–N(1)	2.274(4)	Mn(2)–N(3)	2.248(5)
Mn(1)–N(2)	2.249(4)	Mn(2)–N(4)	2.236(4)
O(1)–Mn(1)–O(2)	56.98(12)	O(5)#1–Mn(2)–O(10)	96.02(15)
O(1)–Mn(1)–O(6)	101.89(15)	O(5)#1–Mn(2)–O(11)	151.78(14)
O(1)–Mn(1)–N(1)	91.62(15)	O(5)#1–Mn(2)–O(12)	87.94(16)
O(1)–Mn(1)–N(2)	151.88(16)	O(5)#1–Mn(2)–N(3)	99.51(16)
O(6)–Mn(1)–O(2)	84.01(14)	O(5)#1–Mn(2)–N(4)	110.32(16)
O(6)–Mn(1)–N(1)	161.44(14)	O(10)–Mn(2)–O(11)	57.73(13)
O(6)–Mn(1)–N(2)	90.36(16)	O(10)–Mn(2)–N(3)	92.40(16)
O(8)–Mn(1)–O(1)	100.70(14)	O(10)–Mn(2)–N(4)	151.33(17)
O(8)–Mn(1)–O(2)	156.97(14)	O(12)–Mn(2)–O(10)	98.30(18)
O(8)–Mn(1)–O(6)	96.62(15)	O(12)–Mn(2)–O(11)	86.20(16)
O(8)–Mn(1)–N(1)	93.25(15)	O(12)–Mn(2)–N(3)	166.28(16)
O(8)–Mn(1)–N(2)	102.93(16)	O(12)–Mn(2)–N(4)	93.89(18)
N(1)–Mn(1)–O(2)	92.99(14)	N(3)–Mn(2)–O(11)	92.34(15)
N(2)–Mn(1)–O(2)	100.09(15)	N(4)–Mn(2)–N(3)	72.76(17)
N(2)–Mn(1)–N(1)	72.09(16)	N(4)–Mn(2)–O(11)	97.61(16)

[a] Symmetry transformations used to generate equivalent atoms: #1 –*x*, –*y*, –*z* + 1; #2 *x*, –*y*, *z* + 1/2; #3 –*x*, *y*, –*z* + 3/2; #4 *x*, *y* – 1, *z*. [b] Symmetry transformations used to generate equivalent atoms: #1 –*x* + 1, –*y*, –*z* + 2; #2 –*x* + 1, –*y*, –*z* + 1. [c] Symmetry transformations used to generate equivalent atoms: #1 *x* – 1, *y* + 1, *z* + 1; #2 *x* + 1, *y* – 1, *z* – 1.

samples using a Quantum Design MPMS SQUID magnetometer. The experimental susceptibilities were corrected for the sample holder and the diamagnetism contributions estimated from Pascal's constants.

Synthesis of $[Mn(oba)(4,4'\text{-bpy})]_n \cdot n(4,4'\text{-bpy})$ (1): A mixture of H_2oba (0.026 g, 0.1 mmol), $Mn(OAc)_2 \cdot 4H_2O$ (0.024 g, 0.1 mmol), 4,4′-bpy·$2H_2O$ (0.019 g, 0.1 mmol), NaOH solution (0.3 mL, 0.65 M) and deionized water(5 mL) was sealed in a Teflon-lined stainless-steel vessel (25 mL) and heated at 180 °C for 72 h. The vessel was then cooled slowly to room temperature. Yellow crystals were isolated by filtration, and washed with water and ethanol. Yield: 0.011 g (17.6%). $C_{34}H_{24}MnN_4O_5$ (623.51): calcd. C 65.44, H 3.85, N 8.98; found C 65.82, H 3.93, N 8.80. IR (KBr pellet): $\tilde{\nu}$ = 3439 cm^{-1} (s), 3072 (w), 1648 (m), 1602 (s), 1560 (m), 1532 (m), 1496 (w), 1413 (m), 1386 (s), 1240 (s), 1159 (m), 1097 (w), 1071 (w), 1011 (w), 879 (w), 803 (m), 785 (m), 695 (w).

Synthesis of $[Mn(oba)(phen)(H_2O)]_n$ (2): The synthesis of complex **2** followed a similar procedure as for complex **1** but with phen·H_2O (0.020 g, 0.1 mmol) instead of 4,4′-bpy·$2H_2O$. Yield: 0.040 g (78.5%). $C_{26}H_{18}MnN_2O_6$ (509.36): calcd. C 61.25, H 3.53, N 5.50; found C 60.88, H 3.67, N 5.53. IR (KBr pellet): $\tilde{\nu}$ = 3317 cm^{-1} (m), 3049 (w), 1602 (s), 1553 (m), 1519 (m), 1496 (m), 1429 (m), 1384 (s), 1335 (s), 1238 (s), 1160 (m), 1137 (w), 1102 (w), 1047 (w), 1011 (w), 876 (w), 849 (m), 786 (m), 698 (w).

Synthesis of $[Mn_2(oba)_2(2,2'\text{-bpy})_2(H_2O)_2]_n \cdot nH_2oba$ (3): The synthesis of complex **3** followed a similar procedure as for complex **1** but with 2,2′-bpy (0.016 g, 0.1 mmol) instead of 4,4′-bpy·$2H_2O$. Yield: 0.032 g (52.1%). $C_{62}H_{46}Mn_2N_4O_{17}$ (1228.9): calcd. C 60.59, H 3.74, N 4.56; found C 60.38, H 3.84, N 4.81. IR (KBr pellet): $\tilde{\nu}$ = 3462 cm^{-1} (m), 3044 (w), 1596 (s), 1565 (m), 1499 (w), 1401 (s), 1316 (w), 1229 (s), 1165 (m), 1100 (w), 1061 (w), 1016 (w), 877 (m), 783 (m), 764 (m), 644 (w).

Synthesis of $[Mn_2(cca)_2(4,4'\text{-bpy})_2]_n \cdot 2n(4,4'\text{-bpy})$ (4): A mixture of H_2cca (0.02 g, 0.1 mmol), $Mn(OAc)_2 \cdot 4H_2O$ (0.024 g, 0.1 mmol), 4,4′-bpy·$2H_2O$ (0.038 g, 0.2 mmol), NaOH solution (0.3 mL, 0.65 M) and deionized water (5 mL) was sealed in a Teflon-lined stainless-steel vessel (25 mL) and heated at 140 °C for 72 h. The vessel was then cooled slowly to room temperature. Yellow crystals were isolated by filtration, and washed with water and ethanol. Yield: 0.020 g (35.9%). $C_{60}H_{44}Mn_2N_8O_8$ (1114.9): calcd. C 64.58, H 3.95, N 10.05; found C 64.20, H 4.12, N 9.97. IR (KBr pellet): $\tilde{\nu}$ = 3442 cm^{-1} (s), 1638 (m), 1588 (s), 1550 (s), 1492 (m), 1417 (m),

Table 4. Selected bond lengths [Å] and angles [°] for complexes **4**–**6**.

4[a]			
Mn(1)–O(1)	2.173(3)	Mn(2)–O(2)	2.166(2)
Mn(1)–O(3)#1	2.152(2)	Mn(2)–O(4)#2	2.197(3)
Mn(1)–N(1)	2.278(3)	Mn(2)–N(2)#6	2.299(3)
O(1)–Mn(1)–N(1)	87.10(10)	O(2)–Mn(2)–O(2)#4	180.0
O(1)–Mn(1)–N(1)#3	92.90(10)	O(2)–Mn(2)–O(4)#2	89.43(10)
O(1)#3–Mn(1)–O(1)	180.0	O(2)–Mn(2)–O(4)#5	90.57(9)
O(3)#1–Mn(1)–O(1)	91.57(10)	O(2)–Mn(2)–N(2)#6	88.95(11)
O(3)#1–Mn(1)–O(1)#3	88.43(10)	O(2)–Mn(2)–N(2)#7	91.05(11)
O(3)#1–Mn(1)–O(3)#2	180.0	O(4)#2–Mn(2)–O(4)#5	179.998(1)
O(3)#1–Mn(1)–N(1)	91.76(10)	O(4)#2–Mn(2)–N(2)#6	86.45(10)
O(3)#1–Mn(1)–N(1)#3	88.24(10)	O(4)#2–Mn(2)–N(2)#7	93.55(11)
N(1)#3–Mn(1)–N(1)	180.0	N(2)#6–Mn(2)–N(2)#7	180.0
5[b]			
Mn(1)–O(1)	2.094(3)	Mn(1)–N(1)	2.317(4)
Mn(1)–O(2)#2	2.203(3)		
O(1)–Mn(1)–O(1)#1	113.4(2)	O(2)#2–Mn(1)–O(2)#3	168.3(2)
O(1)–Mn(1)–O(2)#2	86.1(1)	O(2)#2–Mn(1)–N(1)	85.6(1)
O(1)–Mn(1)–O(2)#3	100.3(1)	O(2)#3–Mn(1)–N(1)	84.9(1)
O(1)–Mn(1)–N(1)	87.9(1)	O(2)#2–Mn(1)–N(1)#1	84.9(1)
O(1)–Mn(1)–N(1)#1	158.1(1)	O(2)#3–Mn(1)–N(1)#1	85.6(1)
O(1)#1–Mn(1)–O(2)#2	100.3(1)	N(1)–Mn(1)–N(1)#1	71.4(2)
O(1)#1–Mn(1)–O(2)#3	86.1(1)		
6[c]			
Mn(1)–O(1)	2.12(4)	Mn(1)–O(6)	2.51(2)
Mn(1)–O(2)#3	2.08(2)	Mn(1)–N(1)	2.245(2)
Mn(1)–O(5)	2.15(2)	Mn(1)–N(2)	2.290(2)
O(1)–Mn(1)–O(5)	94.4(1)	O(2)#3–Mn(1)–N(2)	87.8(7)
O(1)–Mn(1)–O(6)	87.3(1)	O(5)–Mn(1)–O(6)	55.2(3)
O(1)–Mn(1)–N(1)	95.0(8)	O(5)–Mn(1)–N(1)	145.1(3)
O(1)–Mn(1)–N(2)	164.4(8)	O(5)–Mn(1)–N(2)	92.1(5)
O(2)#3–Mn(1)–O(1)	101.9(1)	N(1)–Mn(1)–O(6)	91.7(4)
O(2)#3–Mn(1)–O(5)	116.6(5)	N(2)–Mn(1)–O(6)	84.8(7)
O(2)#3–Mn(1)–O(6)	168.6(8)	N(1)–Mn(1)–N(2)	71.86(7)
O(2)#3–Mn(1)–N(1)	94.2(5)		

[a] Symmetry transformations used to generate equivalent atoms: #1 $-x, -y, -z + 1$; #2 $x, y + 1, z$; #3 $-x, -y + 1, -z + 1$; #4 $-x + 1, -y + 1, -z + 1$; #5 $-x + 1, -y, -z + 1$; #6 $x + 1, y, z - 1$; #7 $-x, -y + 1, -z + 2$; #8 $x, y - 1, z$. [b] Symmetry transformations used to generate equivalent atoms: #1 $-x, y, -z + 3/2$; #2 $x, -y, z - 1/2$; #3 $-x, -y, -z + 2$; #4 $-x + 1/2, -y - 1/2, -z + 2$. [c] Symmetry transformations used to generate equivalent atoms: #1 $x + 1/2, y + 1/2, z$; #2 $-x + 1/2, -y + 1/2, -z + 1$; #3 $-x + 1, -y + 1, -z + 1$; #4 $-x, -y + 1, -z$; #5 $x - 1/2, y - 1/2, z$.

1376 (s), 1225 (m), 1074 (w), 1001 (w), 864 (w), 817 (m), 794 (m), 721 (w), 628 (m), 605 (w).

Synthesis of [Mn(cca)(phen)]$_n$ (5): The synthesis of complex **5** followed a similar procedure as for complex **4** except that phen·H_2O (0.020 g, 0.1 mmol) was used instead of 4,4′-bpy·$2H_2O$ and the temperature was 160 °C. Yield: 0.022 g (48.9%). $C_{24}H_{14}MnN_2O_4$ (449.31): calcd. C 62.07, H 3.29, N 6.58; found C 61.75, H 3.43, N 6.86. IR (KBr pellet): $\tilde{\nu}$ = 3439 cm^{-1} (s), 1649 (s), 1606 (m), 1509 (m), 1425 (m), 1381 (s), 1099 (w), 987 (w), 851 (m), 789 (m), 730 (m), 636 (w).

Synthesis of [Mn(cca)(2,2′-bpy)]$_n$·0.25$n$$H_2O$ (6): The synthesis of complex **6** followed a similar procedure as for complex **4** except that 2,2′-bpy (0.016 g, 0.1 mmol) was used instead of 4,4′-bpy·$2H_2O$ and the temperature was 120 °C. Yield: 0.017 g (41.9%). $C_{20}H_{14.50}MnN_2O_{4.25}$ (405.78): calcd. C 59.15, H 3.57, N 6.90; found C 58.91, H 3.81, N 6.82. IR (KBr pellet): $\tilde{\nu}$ = 3431 cm^{-1} (m), 3025 (m), 1646 (s), 1616 (s), 1536 (s), 1473 (m), 1439 (s), 1390 (s), 1312 (m), 1245 (m), 1171 (m), 1098 (w), 1016 (m), 984 (m), 862 (m), 763 (m), 737 (m), 647 (m), 625 (w).

X-ray Crystallographic Study: Diffraction intensities for the six complexes were collected at 293 K on a Bruker SMART 1000 CCD diffractometer employing graphite-monochromated Mo-K_α radiation (λ = 0.71073 Å). Semi-empirical absorption correction was applied using the SADABS program. The structures were solved by direct methods and refined by full-matrix least-squares on F^2 using the SHELXS-97 and SHELXL-97 programs, respectively.[18] Non-hydrogen atoms were refined anisotropically. Hydrogen atoms were placed in geometrically calculated positions. The crystallographic data for complexes **1** to **6** are listed in Table 2, and selected bond lengths and angles in Tables 3 and 4.

CCDC-293769 to -293774 (for **1**–**6**, respectively) contain the supplementary crystallographic data for this paper. These data can be obtained free of charge from the Cambridge Crystallographic Data Centre via www.ccdc.cam.ac.uk/data_request/cif.

Supporting Information (see footnote on the first page of this article): The other three kinds of coordination environments of the Mn^{II} ion in complex **6**.

Acknowledgments

This work was supported by the National Natural Science Foundation of China (grant nos. 20331010, 20501003 and 20490210).

[1] a) E. Q. Gao, S. Q. Bai, Z. He, C. H. Yan, *Inorg. Chem.* **2005**, *44*, 677–682; b) H. Oshio, M. Nihei, S. Koizumi, T. Shiga, H. Nojiri, M. Nakano, N. Shirakawa, M. Akatsu, *J. Am. Chem. Soc.* **2005**, *127*, 4568–4569; c) A. J. Tasiopoulos, W. Wernsdorfer, K. A. Abboud, G. Christou, *Angew. Chem. Int. Ed.* **2004**, *43*, 6338–6342; d) G. Rajaraman, M. Musugesu, E. C. Sanudo, M. Soler, W. Wernsdorfer, M. Helliwell, C. Muryn, J. Raftery, S. J. Teat, G. Christou, E. K. Brechin, *J. Am. Chem. Soc.* **2004**, *126*, 15445–15457; e) D. J. Price, S. R. Batten, B. Moubaraki, K. S. Murray, *Chem. Commun.* **2002**, 762–763; f) S. Wang, M. S. Wemple, H. L. Tsai, K. Folting, J. C. Huffman, K. S. Hagen, D. N. Hendrickson, G. Christou, *Inorg. Chem.* **2000**, *39*, 1501–1513; g) H. Andres, R. Basler, H. U. Gudel, G. Aromi, G. Christou, H. Buttner, B. Ruffle, *J. Am. Chem. Soc.* **2000**, *122*, 12469–12477.

[2] a) K. N. Ferreira, T. M. Iverson, K. Maghlaoui, J. Barber, S. Iwata, *Science* **2004**, *303*, 1831–1838; b) A. W. Rutherford, A. Boussac, *Science* **2004**, *303*, 1782–1784; c) S. Mukhopadhyay, S. K. Mandal, S. Bhaduri, W. H. Armstrong, *Chem. Rev.* **2004**, *104*, 3981–4026; d) G. C. Dismukes, *Chem. Rev.* **1996**, *96*, 2909–2926.

[3] a) K. B. Jensen, E. Johansen, F. B. Larsen, C. J. McKenzie, *Inorg. Chem.* **2004**, *43*, 3801–3803; b) J. Brinksma, R. Hage, J. Kerschner, B. L. Feringa, *Chem. Commun.* **2000**, 537–538; c) W. Zhang, J. L. Loebach, S. B. Wilson, E. N. Jacobsen, *J. Am. Chem. Soc.* **1990**, *112*, 2801–2803.

[4] a) A. Escuer, F. A. Mautner, M. A. S. Goher, M. A. M. Abu-Youssef, R. Vicente, *Chem. Commun.* **2005**, 605–607; b) C. M. Liu, S. Gao, D. Q. Zhang, Y. H. Huang, R. G. Xiong, Z. L. Liu, F. C. Jiang, D. B. Zhu, *Angew. Chem. Int. Ed.* **2004**, *43*, 990–994; c) E. Q. Gao, S. Q. Bai, Y. F. Yue, Z. M. Wang, C. H. Yan, *Inorg. Chem.* **2003**, *42*, 3642–3649; d) M. A. M. Abu-Youssef, A. Escuer, M. A. S. Goher, F. A. Mautner, G. J. Reiß, R. Vicente, *Angew. Chem. Int. Ed.* **2000**, *39*, 1624–1626; e) R. Cortés, M. Drillon, X. Solans, L. Lezama, T. Rojo, *Inorg. Chem.* **1997**, *36*, 677–683; f) G. D. Munno, M. Julve, G. Viau, F. Lloret, J. Faus, D. Viterbo, *Angew. Chem. Int. Ed. Engl.* **1996**, *35*, 1807.

[5] a) Y. Z. Zhang, S. Gao, Z. M. Wang, G. Su, H. L. Sun, F. Pan, *Inorg. Chem.* **2005**, *44*, 4534–4545; b) F. Karadas, E. J. Schelter, A. V. Prosvirin, J. Bacsa, K. R. Dunbar, *Chem. Commun.* **2005**, 1414–1416; c) R. Lescouëzec, J. Vaissermann, L. M. Toma, R. Carrasco, F. Lloret, M. Julve, *Inorg. Chem.* **2004**, *43*, 2234–2236; d) T. Kashiwagi, S. Ohkoshi, H. Seino, Y. Mizobe, K. Hashimoto, *J. Am. Chem. Soc.* **2004**, *126*, 5024–5025; e) M. Ohha, N. Usuki, N. Fukita, H. Ōkawa, *Angew. Chem. Int. Ed.* **1999**, *38*, 1795–1798.

[6] a) E. Coronado, J. R. Galán-Mascarós, C. J. Gómez-García, C. Martí-Gastaldo, *Inorg. Chem.* **2005**, *44*, 6197–6202; b) E. Coronado, J. R. Galán-Mascarós, C. J. Gómez-García, V. Laukhin, *Nature* **2000**, *408*, 447–449; c) R. Pellaux, H. W. Schmalle, R. Huber, P. Fischer, T. Hauss, B. Ouladdiaf, S. Decurtins, *Inorg. Chem.* **1997**, *36*, 2301–2308; d) S. G. Carling, C. Mathonière, P. Day, K. M. A. Malik, S. J. Coles, M. B. Hursthouse, *J. Chem. Soc., Dalton Trans.* **1996**, 1839–1843.

[7] a) Z. B. Han, X. N. Cheng, X. M. Chen, *Cryst. Growth Des.* **2005**, *5*, 695–700; b) Y. Z. Zheng, G. F. Liu, B. H. Ye, X. M. Chen, *Z. Anorg. Allg. Chem.* **2004**, *630*, 296–300; c) Y. B. Wang, Z. M. Wang, C. H. Yan, L. P. Jin, *J. Mol. Struct.* **2004**, *692*, 177–186; d) M. Kondo, Y. Irie, Y. Shimizu, M. Miyazawa, H. Kawaguchi, A. Nakamura, T. Naito, K. Maeda, F. Uchida, *Inorg. Chem.* **2004**, *43*, 6139–6141; e) X. M. Chen, G. F. Liu, *Chem. Eur. J.* **2002**, *8*, 4811–4817; f) G. F. Liu, Z. P. Qiao, H. Z. Wang, X. M. Chen, G. Yang, *New J. Chem.* **2002**, *26*, 791–795; g) J. Tao, J. X. Shi, M. L. Tong, X. X. Zhang, X. M. Chen, *Inorg. Chem.* **2001**, *40*, 6328–6330.

[8] H. Kumagai, Y. Oka, K. Inoue, M. Kurmoo, *J. Chem. Soc., Dalton Trans.* **2002**, 3442–3446.

[9] a) X. Q. Lu, J. J. Jiang, C. L. Chen, B. S. Kang, C. Y. Su, *Inorg. Chem.* **2005**, *44*, 4515–4521; b) B. Q. Ma, K. L. Mulfort, J. T. Hupp, *Inorg. Chem.* **2005**, *44*, 4912–4914; c) R. Pothiraja, M. Sathiyendiran, R. J. Butcher, R. Murugavel, *Inorg. Chem.* **2005**, *44*, 6314–6323; d) S. Kraft, E. Hanuschek, R. Beckhaus, D. Haase, W. Saak, *Chem. Eur. J.* **2005**, *11*, 969–978; e) M. I. Khan, E. Yohannes, R. C. Nome, S. Ayesh, V. O. Golub, C. J. O'Connor, R. J. Doedens, *Chem. Mater.* **2004**, *16*, 5273–5279; f) R. Lin, J. H. K. Yip, K. Zhang, L. L. Koh, K. Y. Wong, K. P. Ho, *J. Am. Chem. Soc.* **2004**, *126*, 15852–15869.

[10] a) B. Gómez-Lor, E. Gutiérrez-Puebla, M. Iglesias, M. A. Monge, C. Ruiz-Valero, N. Snejko, *Chem. Mater.* **2005**, *17*, 2568–2573; b) F. Li, Z. Ma, Y. L. Wang, R. Cao, W. H. Bi, X. Li, *CrystEngComm* **2005**, *7*, 569–574; c) B. H. Ye, M. L. Tong, X. M. Chen, *Coord. Chem. Rev.* **2005**, *249*, 545–565; d) X. L. Wang, C. Qin, E. B. Wang, L. Xu, Z. M. Su, C. W. Hu, *Angew. Chem. Int. Ed.* **2004**, *43*, 5036–5040; e) N. Hao, E. H. Shen, Y. G. Li, E. B. Wang, C. W. Hu, L. Xu, *Eur. J. Inorg. Chem.* **2004**, 4102–4107; f) L. Y. Zhang, G. F. Liu, S. L. Zheng, B. H. Ye, X. M. Zhang, X. M. Chen, *Eur. J. Inorg. Chem.* **2003**, 2965–2971.

[11] C. Y. Sun, L. P. Jin, *J. Mol. Struct.* **2005**, *733*, 63–68.
[12] W. Wojciechowski, *Inorg. Chim. Acta* **1967**, *1*, 318.
[13] a) H. Iikura, T. Nagata, *Inorg. Chem.* **1998**, *37*, 4702–4711; b) J. Kim, J. M. Lim, M. C. Suh, H. Yun, *Polyhedron* **2001**, *20*, 1947–1951.
[14] a) Z. H. Ni, H. Z. Kou, L. Zheng, Y. H. Zhao, L. F. Zhang, R. J. Wang, A. L. Cui, O. Sato, *Inorg. Chem.* **2005**, *44*, 4728–4736; b) G. A. van Albada, A. Mohamadou, W. L. Driessen, R. Gelder, S. Tanase, J. Reedijk, *Polyhedron* **2004**, *23*, 2387–2391.
[15] Oxygen Contamination, MPMS Application Note 1014–210, *Quantum Design*, **1997**.
[16] R. L.Carlin, *Magnetochemistry*, Springer-Verlag, **1986**, p170.
[17] S. Durot, C. Policar, G. Pelosi, F. Bisceglie, T. Mallah, J. P. Mahy, *Inorg. Chem.* **2003**, *42*, 8072–8080.
[18] G. M. Sheldrick, *SHELXTL-97*, *Program for the Refinement of Crystal Structures*, University of Göttingen, Germany, **1997**.
Received: December 30, 2005
Published Online: April 18, 2006

